Hybrid Integrator-Gain System for Active Vibration Isolation with Improved Transient Response

Marcel Heertjes [*,**] **Sebastiaan van den Eijnden** [*] **Bardia Sharif** [*]
Maurice Heemels [*] **Henk Nijmeijer** [*]

[*] *Mechanical Engineering Department, Eindhoven University of Technology, The Netherlands.*
[**] *Mechatronics System Design Department, ASML, The Netherlands (e-mail m.f.heertjes@tue.nl).*

Abstract: In this paper a linear bandpass filter is compared to a hybrid integrator-gain based bandpass filter regarding its usefulness in active vibration isolation. Vibration isolation refers to a form of skyhook damping in which a velocity output signal from a system having structural dynamics is fed back to a controller, the latter having bandpass characteristics. At those frequencies where the controller passes the input signal (after gain multiplication) a force proportional to velocity is obtained that can be used to provide active damping to the system, *i.e.*, damping of one (or more) of its structural modes. Outside this frequency band the controller input signal is attenuated, which is often desirable in view of incorrect sensor information at low frequencies and/or to avoid amplification of high-frequency noise. In this context, the use of a hybrid integrator-gain system will be studied regarding its possible phase advantages compared to linear integrators. These advantages stem from the control design itself, in the sense that by design the control output force signal and the input velocity error signal have equal sign. In the context of vibration control, an enhanced transient (closed-loop) response is obtained, *i.e.*, less overshoot and reduced settling times, but at the cost of increased rise times.

1. INTRODUCTION

The traditional trade-off between (a) enhanced low-frequency disturbance suppression, and (b) a desired transient response using linear integral control (Feuer et al., 1997) forms an excellent showcase for hybrid integrator-gain systems (Deenen et al., 2017), or further abbreviated as HIGS. HIGS consist of an integrator mode and a gain mode that together with switching logic guarantee that the input and output of the hybrid integrator are of equal sign. Despite the fact that the concept of phase is only well-defined for linear systems, HIGS have a clear phase advantage over linear integrators. Namely from quasi-linear frequency domain analysis, it follows that the phase lag associated with HIGS does not exceed 38.15 degrees. This value is also found with first-order reset elements that originate from Clegg's integrator (Beker et al., 2004; Zaccarian et al., 2011; Van Loon et al., 2017). Reset controllers achieve this nice phase behavior by discontinuous control signals, while the HIGS induces continuous control outputs.

In terms of performance, a control design based on HIGS can be particularly useful in high-precision mechatronic systems, *e.g.*, the control of wafer scanners used in the production of microchips (Oomen et al., 2014). In such systems reduced phase lag can be used to enhance frequency-domain characteristics like bandwidth giving improved low-frequency disturbance rejection properties of the closed-loop system, see for example Heertjes et al. (2018) for an experimental demonstration. In this paper, however, HIGS is used to improve the (time-domain) transient response (Zheng et al., 2000). In the context of active vibration isolation, *i.e.*, skyhook damping of resonances related to suspension (or structural) modes, the phase advantages associated with HIGS can be exploited, as we will show, to improve properties like overshoot and settling times.

Next to performance analysis, stability of the closed-loop hybrid system can, for example, be studied using a linear matrix inequality (LMI) based approach for the case of having multiple nonlinearities, which can be seen as a non-trivial extension of the work by Nešić et al. (2008) and Aangenent et al. (2009). In this regard, we also would like to mention the works of Beker et al. (2004) and Carrasco et al. (2010) for other interesting approaches in the context of reset control systems. In this paper, however, we will use a passivity-based argument in a Lyapunov-like context similar to Van Loon et al. (2017); Deenen et al. (2017).

The main contribution of this paper is the introduction of a HIGS bandpass filter. In active vibration isolation when damping suspension modes (often through skyhook damping, see, for example, Li & Goodall (1999)) linear bandpass filters are frequently used either on direct velocity measurements, for example with geophones, or on the integrated output of accelerometers as in Van der Poel et al. (2007); Tjepkema et al. (2011). In such cases, a bandpass filter operation allows for skyhook damping – gain multiplied with a velocity input (Preumont, 2011) – in a limited frequency band while avoiding (a) low-frequency deterioration of the passive isolation properties due to poor sensor information, and (b) high-frequency sensitivity of the closed-loop system in the presence of noise. To mimic a bandpass operation, the HIGS-based bandpass filter features a series connection of two nonlinear filters. In the first filter, the output of one HIGS is subtracted from unity feedthrough thereby generating a nonlinear filter operation with highpass properties. In the second filter, a sole HIGS is used, which has lowpass properties. As a second contribution, comparison studies are conducted in which skyhook damping is applied through numerical simulations by using either a linear bandpass filter or a HIGS bandpass filter. Three well-known transient performance measures are evaluated being overshoot, settling

time, and rise time (Skogestad & Postlethwaite, Section 2.4.2, 2005).

The remainder of the paper is organized as follows. In Section 2, a small introduction is given on HIGS. In Section 3, the HIGS bandpass filter is introduced, which, in Section 4, will be used in an active vibration control setting as a means to provide skyhook damping. In Section 5, simulation results are discussed for parameter studies involving a range of skyhook damping values. In Section 6, conclusions and recommendations are given for further research particularly in the direction of HIGS-based control design.

2. HYBRID INTEGRATOR-GAIN SYSTEM

The hybrid integrator-gain system $\mathscr{H}$ (or HIGS) is given by the following state-space representation of its differential-algebraic equations:

$$\mathscr{H}(e,u,\dot{e}) := \begin{cases} \dot{x}_h = \omega_h e, & \text{if } (e,u,\dot{e}) \in \mathscr{F}_1 \quad (1a) \\ x_h = k_h e, & \text{if } (e,u,\dot{e}) \in \mathscr{F}_2 \quad (1b) \\ u = x_h, & \quad (1c) \end{cases}$$

with state $x_h \in \mathbb{R}$, input $e \in \mathbb{R}$ with corresponding time derivative $\dot{e} \in \mathbb{R}$, control output $u \in \mathbb{R}$, parameters $\omega_h \in [0,\infty)$ and $k_h \in (0,\infty]$ representing the integrator frequency and gain value, respectively, and with $\mathscr{F}_1$ and $\mathscr{F}_2$ denoting the regions where the different subsystems are active. The input signal e is assumed to be continuous and piecewise differentiable. Moreover, the initial condition is assumed to be zero, *i.e.*, $x_h(0) = 0$. $\mathscr{H}$ in (1) is input amplitude independent and designed to mainly operate in integrator mode (1a). Its input-output relation, however, is constrained to a $[0,k_h]$-sector when $(e,u,\dot{e}) \in \mathscr{F}$, where

$$\mathscr{F} := \left\{ (e,u,\dot{e}) \in \mathbb{R}^3 \mid eu \geq \frac{1}{k_h} u^2 \right\}. \quad (2)$$

When the integrator dynamics (1a) tend to violate the sector constraint, a switch to the gain mode dynamics (1b) is enforced, leading to the definition of subset $\mathscr{F}_2$. The resulting sets are defined by

$$\mathscr{F}_1 := \mathscr{F} \setminus \mathscr{F}_2, \quad (3)$$

$$\mathscr{F}_2 := \left\{ (e,u,\dot{e}) \in \mathscr{F} \mid u = k_h e \ \wedge \ \omega_h e^2 > k_h \dot{e} e \right\}. \quad (4)$$

Note that the condition $\omega_h e^2 > k_h \dot{e} e$ implies that $\dot{u}$ in gain mode is smaller than $\dot{u}$ in integrator mode, in which case the system is constrained to gain mode to avoid sector violation.

Apart from the time-domain properties of $\mathscr{H}$ resulting from (1), its frequency-domain properties can be studied by describing function analysis. Consider $e(\tau)$ to be a sinusoidal input:

$$e(\tau) = \hat{e}\sin(\tau), \quad (5)$$

with $\tau = \omega t,\ \omega \geq 0,\ t \in \mathbb{R}_{\geq 0}$ and amplitude $\hat{e} \in \mathbb{R}$. It can be shown, see Heertjes et al. (2018), that the describing function $\mathscr{D}(j\omega) \in \mathbb{C}$ of $\mathscr{H}$ in (1) between input e and output u is given by

$$\mathscr{D}(j\omega) = \frac{a_1 + b_1 j}{\hat{e}}, \quad (6)$$

where $a_1, b_1 \in \mathbb{C}$ are the Fourier coefficients of the fundamental harmonic, which are given by

$$\begin{aligned} a_1 &= \frac{\hat{e}}{2\pi}\left\{ \frac{\omega_h}{\omega}\left(\cos(2\gamma) - 4\cos(\gamma) + 3\right) \right. \\ &\qquad \left. + k_h\left(2(\pi-\gamma) + \sin(2\gamma)\right)\right\} \\ b_1 &= \frac{\hat{e}}{2\pi}\left\{ \frac{\omega_h}{\omega}\left(4\sin(\gamma) - \sin(2\gamma) - 2\gamma\right) \right. \\ &\qquad \left. - k_h\left(1 - \cos(2\gamma)\right)\right\}, \end{aligned} \quad (7)$$

and where the switch instant γ is defined by

$$\gamma = 2\arctan(\omega k_h/\omega_h). \quad (8)$$

Note that $\gamma \to \pi$ gives

$$\lim_{\gamma\to\pi} \mathscr{D}(j\omega) = \frac{\omega_h}{j\omega}\left\{1 + \frac{4j}{\pi}\right\}, \quad (9)$$

which resembles a 20dB/decade amplitude decay similar to a linear integrator, but with a phase lag of only ≈ 38.15 degrees due to the extra imaginary-valued constant $4/\pi$. It is essentially this phase advantage over linear systems that we want to exploit in HIGS-based control design for improved transient response.

3. HIGS-BASED BANDPASS FILTER DESIGN

Before presenting the HIGS-based bandpass filter design, first consider the following linear bandpass filter in Laplace domain:

$$\mathscr{C}_{bp}(s) = \frac{u(s)}{e(s)} = \overbrace{\frac{\omega_{lp}}{s+\omega_{lp}}}^{lowpass} \cdot \underbrace{\frac{s}{s+\omega_{hp}}}_{highpass}, \quad (10)$$

with $\omega_{hp} = 2\pi \times 0.1$ rad$\cdot$s^{-1} and $\omega_{lp} = 2\pi \times 10$ rad$\cdot$s^{-1} the filter's cut-off frequencies. In (10), ω_{hp} is chosen at a frequency beyond which the sensor information becomes valid. $\omega_{lp} > \omega_{hp} > 0$ can be used to reduce the sensitivity of the closed-loop system to noise by lowering the gain at high frequencies. Note that in the interval $[\omega_{hp}, \omega_{lp}]$, (10) approximates unity gain.

Given (10), consider the block diagram in Fig.1, which represents the hybrid bandpass filter $\mathscr{H}_{bp}$, *i.e.*, the HIGS-based equivalent of (10) with $\mathscr{H}_1, \mathscr{H}_2$ from (1) with $k_{h,1} = k_{h,2} = 1$, $\omega_{h,1} = \omega_{hp}/(2\alpha)$ rad$\cdot$s^{-1}, $\omega_{h,2} = \omega_{lp}/\alpha$ rad$\cdot$s^{-1}, and $\alpha = |1 + 4j/\pi|$ a scaling constant that follows from (9).

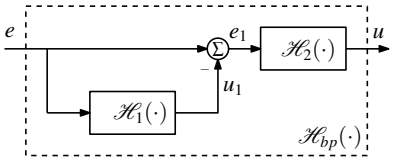

Fig. 1. Block diagram of a HIGS-based bandpass filter.

To illustrate the behavior of both bandpass filters, *i.e.*, $\mathscr{C}_{bp}$ and $\mathscr{H}_{bp}$, consider the time responses as shown in Fig. 2, which are the result of a sinusoidal input as in (5) with $\hat{e} = 1$ and with $\omega \in \{2\pi \times 1/20, 2\pi, 2\pi \times 20\}$ rad$\cdot$s^{-1} (gray curves). First observe that by choice of its parameter $\omega_{h,1}$, the integrator in $\mathscr{H}_1$ is fast enough to invoke the integrator mode for the case $\omega = 2\pi \times 1/20$ rad$\cdot$s^{-1}, which is shown in the upper part of the figure. At $t \approx 6.4$ seconds, $\mathscr{H}_1$ switches from integrator mode to gain mode, which means its output becomes equal to its input e, *i.e.*, the input to $\mathscr{H}_2$ becomes zero, which subsequently yields the output u to be zero too. At $t = 10$ seconds, e changes sign and $\mathscr{H}_1$ switches back to integrator mode. For the cases $\omega = 2\pi$ rad$\cdot$s^{-1} and $\omega = 2\pi \times 20$ rad$\cdot$s^{-1}, the input signal to $\mathscr{H}_2$, *i.e.*, $e - k_{h,1}\mathscr{H}_1(e,u,\dot{e}) \approx e$, reflects a too slow contribution of $\mathscr{H}_1$. Conversely, by choice of its parameter $\omega_{h,2}$, the integrator in $\mathscr{H}_2$ is too fast for the cases $\omega = 2\pi \times 1/20$ rad$\cdot$s^{-1} and $\omega = 2\pi$ rad$\cdot$s^{-1}. As a result, $\mathscr{H}_2$ largely operates in gain mode. For the case $\omega = 2\pi$ rad, *i.e.*, the middle part of the figure, this means that since $e - k_{h,1}\mathscr{H}_1(e,u,\dot{e}) \approx e$ by virtue of $\mathscr{H}_1$ and because $\mathscr{H}_2 \approx 1$, the output $u \approx e$. For the case $\omega = 2\pi \times 20$ rad$\cdot$s^{-1}, *i.e.*, the lower part of the figure, it can be seen that for $t \in [0.05, 0.07]$ seconds, $\mathscr{H}_2$ operates

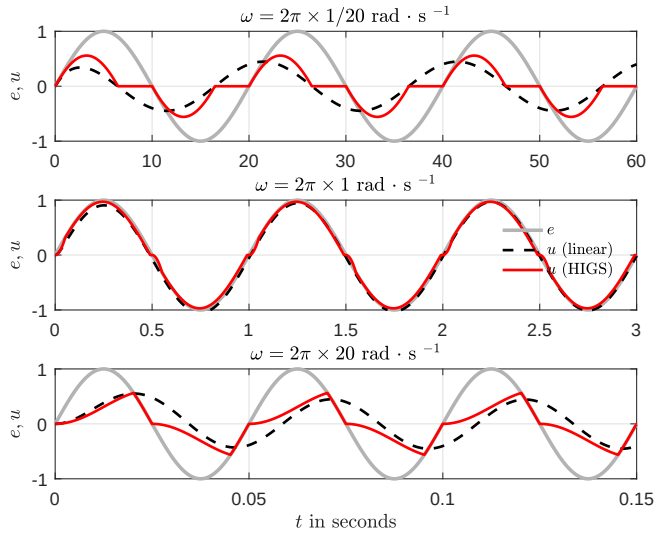

Fig. 2. Time series simulations of the output u of a linear bandpass filter in (10) (dashed-black) and the HIGS-based bandpass filter from Fig. 1 (red) to a sinusoidal input e (gray) with $\omega \in \{2\pi \times 1/20, 2\pi, 2\pi \times 20\}$ rad $\cdot$ s^{-1}.

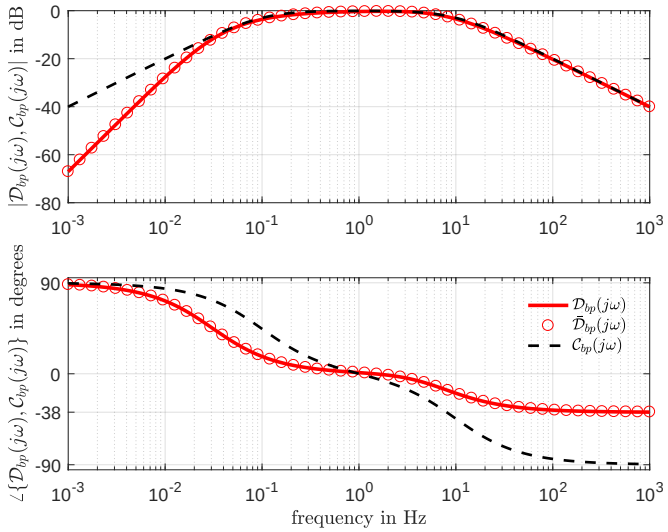

Fig. 3. Bode diagram of linear bandpass filter $\mathscr{C}_{bp}(j\omega)$ (dashed black) and the describing function of the HIGS-based bandpass filter $\mathscr{D}_{bp}(j\omega)$ (red).

in integrator mode, whereas during $t \in (0.07, 0.08)$ seconds, it operates in gain mode. For all responses, observe that the hybrid behavior of the HIGS-based bandpass filter (red curves) effectively results in mimicking either phase lead (upper part) or phase lag (lower part) while avoiding unequal signs of the pair (e,u). The latter is clearly not the case for the response of the linear bandpass filter (dashed black curves). It can also be observed that the maximum absolute values of the responses, *i.e.*, $\|u\|_\infty$, are similar for $\mathscr{H}_{bp}$ and $\mathscr{C}_{bp}$. As a final observation, note that the linear responses include a transient effect that is clearly gone (by design) in the HIGS-based responses as soon as e crosses zero, *i.e.*, in Fig. 2 $e(0) = 0$.

In frequency domain, the HIGS-based bandpass filter can be evaluated in an approximate manner using the following describing function [1]:

$$\mathscr{D}_{bp}(j\omega) \approx (1 - \mathscr{D}_1(j\omega))\mathscr{D}_2(j\omega), \tag{11}$$

where $\mathscr{D}_1(j\omega), \mathscr{D}_2(j\omega)$ follow from (6) and (7) with the parameter values given in the discussion part of Fig 1. Note that (11) does not necessarily represent the true describing function $\bar{\mathscr{D}}_{bp}$ of $\mathscr{H}_{bp}$ but gives an approximation. The approximation, however, is in full accordance with the earlier observations that

$$\begin{aligned} \lim_{\omega \to 0} \bar{\mathscr{D}}_{bp}(j\omega) &= (1 - \mathscr{D}_1(j\omega)) \text{ and} \\ \lim_{\omega \to \infty} \bar{\mathscr{D}}_{bp}(j\omega) &= \mathscr{D}_2(j\omega). \end{aligned} \tag{12}$$

The frequency response functions of $\mathscr{D}_{bp}(j\omega)$ from (11), the true describing function $\bar{\mathscr{D}}_{bp}(j\omega)$ derived from time-series simulations and the computation of the first Fourier coefficients, and $\mathscr{C}_{bp}(j\omega)$ from (10) are depicted in the Bode diagram of Fig. 3. First, it can be observed that $\mathscr{D}_{bp}(j\omega)$ represents an excellent approximation of $\bar{\mathscr{D}}_{bp}(j\omega)$. At low frequencies, $\mathscr{D}_{bp}(j\omega)$ induces 20 dB/decade extra decay compared to the linear first-order highpass filter in (10) but with having a similar phase lead of 90 degrees, *i.e.*, a clear manifestation of defying Bode's gain-phase relation. From a mathematical perspective, this behavior can be understood by considering the limit case of $1 - \mathscr{D}_1(j\omega)$ for $\omega \to 0$, *i.e.*,

$$\lim_{\omega \to 0} (1 - \mathscr{D}_1(j\omega))) = \lim_{\omega \to 0} \left(\frac{16\alpha^2}{3\pi} \frac{\omega^2}{\omega_{hp}^2} j \right), \tag{13}$$

which, being a purely positive imaginary number proportional to ω^2, explains the observed 40 dB/decade amplification and 90 degrees phase lead. Second, in the interval $\omega \in 2\pi \cdot [0.1, 10]$ rad $\cdot$ s^{-1}, both filters attempt at passing through unity gain. The linear filter $\mathscr{C}_{bp}(j\omega)$, however, exhibits inferior phase characteristics compared to $\mathscr{D}_{bp}(j\omega)$. Third, for $\omega \to \infty$ it follows that $\mathscr{D}_{bp}(j\omega) \to \mathscr{D}_2(j\omega)$, hence (12), thereby inducing 51.85 degrees less phase lag than its linear counterpart $\mathscr{C}_{bp}(j\omega)$.

4. ACTIVE VIBRATION ISOLATION USING HIGS-BASED SKYHOOK DAMPING

The favorable properties of a HIGS-based bandpass filter design, as discussed in the previous section, are used in this section in the context of active vibration isolation. In particular, a skyhook damping control strategy will be studied that attempts at improving the dynamics associated with a weakly damped suspension mode. A simple second-order mass-damper-spring system will be used that in its essence is encountered in many engineering applications, for example, the active vibration isolation system as considered in Beijen et al. (2018) and which is used in the wafer scanning industry to isolate the optics and measurement systems.

For a second-order mass-damper-spring system with mass m, damping coefficient b, and stiffness coefficient k, the control schematics are depicted in the right part of Fig.4 while a mechanical analogy is given in the left part of the figure. Output y denotes the displacement of the payload, while $\dot{y}$ denotes the corresponding 'skyhook' velocity, which is obtained (after integration) by measurement using an accelerometer placed atop the payload. The mass-damper-spring system is supported by a structure whose displacement is denoted by x. This structure is assumed to be rigid and independent from whatever forces are being exerted on it, be it spring forces $F_k = ky - kx$, damper forces $F_b = b\dot{y} - b\dot{x}$, or control forces F_c. To obtain skyhook

[1] For a HIGS element $\mathscr{H}$, it can be shown that at least 94% of its output power associates with the fundamental harmonic thereby limiting the possibly detrimental effects of higher harmonics in the excitation of structural modes.

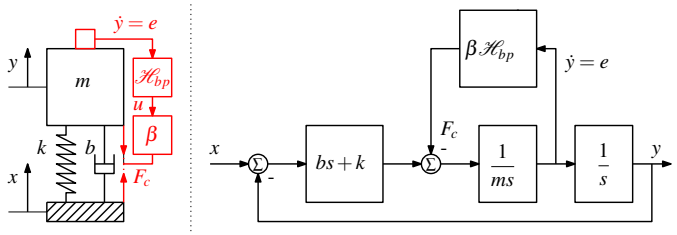

Fig. 4. Block diagram of a HIGS-based skyhook damper design applied to a mass-damper-spring system (right part of the figure) along with its mechanical analogy (left part of the figure).

damping, the control forces F_c, which are applied to the payload, for instance, by using linear synchronous motors (LSMs), feature the multiplication of the signal u with a skyhook gain β, *i.e.*, $F_c = \beta u$. Herein, u represents the bandpass filtered velocity $\dot{y}$, which, in accordance to earlier notation, equals $\dot{y} := e$, with e the control input of the bandpass filters, *i.e.*, (10) for the linear filter $\mathscr{C}_{bp}(s)$ and Fig.1 for the HIGS filter operation $\mathscr{H}_{bp}(e,u,\dot{e})$.

In frequency-domain, the transfer from input x to output y, also known as the transmissibility function, often expresses the sensitivity of an isolated payload to floor vibrations. That is, if the mass-damper-spring system is considered to be simply mounted to the floor. To accommodate for the nonlinear case, where a frequency response function description does not exist, we define the magnitudes of the transmissibility function as ratios of the root-mean-square (RMS) values of the steady-state periodic responses $y(t) = y(t+T)$ over period time $T = 2\pi/\omega > 0$ divided by the RMS-values of an harmonic input $x(t) = x(t+T) = \sin(\omega t)$. Note that we have not guaranteed periodicity of y, for example, by guaranteeing the closed-loop system with HIGS to be convergent. At this point, we assume that every periodic input $x(t) = x(t+T)$ induces a unique periodic response $y(t) = y(t+T)$ with the same period time T. Since

$$\sqrt{\frac{1}{T}\int_0^T \sin^2(2\pi t/T)dt} = \frac{1}{2}\sqrt{2}, \tag{14}$$

for all $T > 0$, the nonlinear transmissibility function $\bar{T}$ in terms of magnitude can be defined as

$$\bar{T}(\omega) = \sqrt{\frac{2}{T}\int_0^T y^2(t)dt},\ T = \frac{2\pi}{\omega} > 0. \tag{15}$$

Note that for the linear case, this definition yields identical magnitude characteristics as obtained from the corresponding frequency response functions $\tilde{T}(j\omega) = y(j\omega)/x(j\omega)$. Also note that for the nonlinear case, (15) represents an alternative to describing function analysis in which the full nonlinear response is considered including all harmonics, However, (15) no longer provides any phase information. Given (15), the magnitude plot of the transmissibility function is shown in Fig. 5. In this figure, three cases are considered: (a) the passive system with no control force, *i.e.*, $F_c(t) = 0$ (gray), (b) the linear skyhook damped system with $F_c(s) = \mathscr{C}_{bp}(s)e(s)$ (black), and (c) the HIGS-based skyhook damped system with $F_c(t) = \mathscr{H}_{bp}(e(t))$ (red). It can be seen that with a skyhook dimensionless (active) damping coefficient of $\bar{\zeta} = \beta/(2m\sqrt{k/m}) = 1$ both linear and HIGS-based control designs seemingly achieve identical damping in their steady-state responses, which can be efficiently computed using the mixed time-frequency-domain algorithm from Pavlov et al. (2013). The latter, under the assumption that the closed-loop system is convergent. Note that the small deterioration in transmissibility both prior and beyond the resonance frequency such

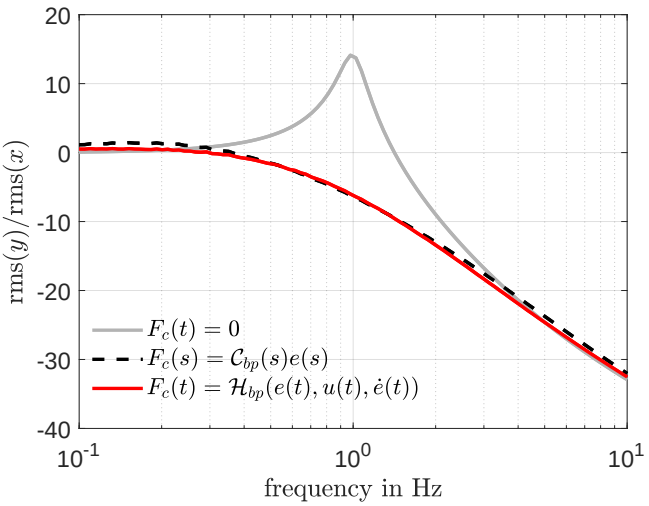

Fig. 5. Nonlinear Bode magnitude plot of (a) the passive system with $F_c(t) = 0$ (gray), (b) the linear skyhook damped system with $F_c(s) = \mathscr{C}_{bp}(s)e(s), \beta = 1$ (black), and (c) the amplitude-independent HIGS-based skyhook damped system with $F_c(t) = \mathscr{H}_{bp}(e(t),u(t),\dot{e}(t)), \beta = 1$ (red); the transmissibility is defined as the ratio of the RMS-values of the steady-state responses divided by the RMS-values of a sinusoidal input $e = \sin(\omega t)$.

as occurring with the linear control design and being the result of phase lag induced by the high- and low-pass filters does hardly occur with the HIGS-based design. Differences between the linear and the HIGS-based control design are expected to become more pronounced in the transient response, which will be studied in the next section. Before that a few comments are in order given (a) the nonlinear context of the HIGS-based control design in Section 2 and (b) the approximative nature of the describing function analysis in Section 3.

Remark 1. Observe that the closed-loop system presented in Fig. 4 can be rearranged into Lur'e form, in which the linear transfer $\mathscr{G}(s)$ from $-F_c$ to e, given by

$$\mathscr{G}(s) = \frac{e(s)}{-F_c(s)} = \frac{s}{ms^2+bs+k}, \tag{16}$$

is used in feedback with the nonlinear HIGS-based bandpass filter $\mathscr{H}_{bp}(e,u,\dot{e})$. Often, for such systems containing a dynamic nonlinearity in the feedback loop, a circle-criterion-like argument is used for asserting closed-loop stability, see *e.g.*, Van Loon et al. (2017) and Deenen et al. (2017). The key aspects in such an argument are (i) the nonlinearity satisfies a sector constraint, and (ii) the nonlinear element in isolation is input-to-state stable (ISS). For the HIGS bandpass filter such properties can be shown as follows.

By invoking properties of a single HIGS it can be concluded that the HIGS-based bandpass filter satisfies the sector condition

$$u^2 \leq \mathscr{H}_{bp}(e,u,\dot{e})e \leq e^2. \tag{17}$$

Indeed, since by design the output $u_1 = \mathscr{H}_1(e,u_1,\dot{e})$ always has the same sign as the input e and is upper bounded in absolute magnitude by $|e|$, it follows that $e_1 := e - \mathscr{H}_1(e,u_1,\dot{e})$ always has the same sign as e, *i.e.*, $ee_1 \geq 0$. Furthermore, since e_1 is the input to the second HIGS, it follows that $(e - \mathscr{H}_1(e,u_1,\dot{e}))u \geq u^2$ and thus $eu \geq eu - u_1u \geq u^2$ in which the fact is used that $ue_1 \geq 0$, and therefore $u_1u = \mathscr{H}_1(e,u_1,\dot{e})u \geq 0$. The upper bound in (17) follows from the inequality

$$(e - \mathscr{H}_1(e,u_1,\dot{e}))^2 \geq (e - \mathscr{H}_1(e,u_1,\dot{e}))u, \tag{18}$$

and by exploiting the fact that u and $\mathscr{H}_1(e,u_1,\dot{e})$ have equal sign and the magnitude of the second HIGS' output is bounded by its input, that is $|u| \leq |e - \mathscr{H}_1(e,u_1,\dot{e})|$.

ISS of the HIGS bandpass filter in isolation is shown here by first showing that a single HIGS is ISS. Second, it is shown that the combination of two separate Lyapunov functions (each associated with one HIGS element) yields one ISS Lyapunov function for the bandpass filter as a whole.

Lemma 1. The HIGS element as presented in (1) is ISS.

Proof: consider the quadratic function

$$\tilde{S}(x_h) = \frac{1}{2}x_h^2. \tag{19}$$

When (1) operates in the integrator mode, one has

$$\begin{aligned}\dot{\tilde{S}}(x_h) =& \omega_h e x_h \\ =& -\omega_h x_h^2 + \omega_h x_h^2 + \omega_h e x_h \\ \leq& -\omega_h x_h^2 + \omega_h(1+k_h)e^2,\end{aligned} \tag{20}$$

where the last inequality follows from the fact that $e^2 \geq \frac{1}{k_h} eu$. Moreover, when (1) operates in the gain mode, one has

$$\begin{aligned}\dot{\tilde{S}}(x_h) =& x_h k_h \dot{e} = k_h^2 e\dot{e} \\ \leq& k_h \omega_h e^2 = -\omega_h x_h^2 + \omega_h x_h^2 + \omega_h e x_h \\ \leq& -\omega_h x_h^2 + \omega_h(1+k_h)e^2,\end{aligned} \tag{21}$$

where once again the sector condition together with the switching criteria ($u = x_h = k_h e$ and $\omega_h e^2 > k_h \dot{e} e$) have been used. Thus, (20) and (21) yield the same upper bound on the time derivative of $\tilde{S}(x_h)$ along the trajectories of (1). It can therefore be concluded that a HIGS element as presented in (1) is ISS (Sontag & Wang, 1995). □

As shown above, the HIGS admits a quadratic function $\tilde{S}(x_h) = \frac{1}{2}x_h^2$ with time-derivative

$$\dot{\tilde{S}} \leq -\omega_h x_h^2 + \rho e x_h, \tag{22}$$

where $\rho = \omega_h(1+k_h) > 0$. By choosing a function $S(x_{h1},x_{h2}) = \frac{1}{2}(x_{h1}^2 + x_{h2}^2)$, for the interconnection in Fig. 1, (22) leads to

$$\dot{S} \leq -(\omega_{h,1}x_{h1}^2 + \omega_{h,2}x_{h2}^2) + \rho_{12} e x_{h1} + \rho_{12}(e - x_{h1})x_{h2}, \tag{23}$$

with $\rho_{12} = (\omega_{h,1} + \omega_{h,2})(1+k_h)$. One can subsequently use the fact that $x_{h1}x_{h_2} \geq 0$ to conclude

$$\dot{S} \leq -(\omega_{h,1}x_{h1}^2 + \omega_{h,2}x_{h2}^2) + \rho_{12} e(x_{h1} + x_{h2}). \tag{24}$$

Moreover, since by construction of the HIGS, one has $e x_{h2} \leq e(e - x_{h1})$ and thus

$$e(x_{h1} + x_{h2}) \leq e x_{h1} + e(e - x_{h1}) = e^2.$$

As a result, it holds true that

$$\dot{S} \leq -(\omega_{h,1}x_{h1}^2 + \omega_{h,2}x_{h2}^2) + \rho_{12} e^2, \tag{25}$$

i.e., an ISS Lyapunov function for the isolated hybrid band-pass filter $\mathscr{H}_{bp}$ is obtained.

Using the previously discussed properties and by realizing that $\mathscr{G}(s)$ is Hurwitz and strictly positive real, *i.e.*, $\Re\{\mathscr{G}(s)\} \geq 0$ for all $s \in \mathbb{C}$, Theorem 1 in Deenen et al. (2017) can be applied to conclude closed-loop stability for all $\beta > 0$. Remark that, in general, $\mathscr{G}(s)$ will not be positive real, for example in the presence of higher-order dynamics or delays. In that case, an evaluation of $\Re\{\mathscr{G}(s)\} \geq -1/\beta_{max}$ for some $0 < \beta \leq \beta_{max}$ can be performed in order to guarantee closed-loop stability for a subset of values of β. In the case that β_{max} resulting from such an evaluation appears too restrictive for the HIGS-based design to be effective, other options can be surveyed. Among these options are: (i) the introduction of extra filtering of F_c as to obtain more desirable stability properties of $\mathscr{G}(s)$, *i.e.*, loopshaping to obtain $\mathscr{G}^*(s) = \mathscr{G}(s)F_c(s)$, possibly at the loss of performance obtained in the absence of such filtering, *i.e.*, $F_c(s) = 1$, and (ii) studies on piecewise quadratic (or more general) Lyapunov functions. Regarding the latter note that the circle criterion essentially exploits a common quadratic Lyapunov function and in that sense may yield a too conservative assessment of the closed-loop system.

5. TRANSIENT BEHAVIOR

To study the transient behavior of the (nonlinearly) controlled mass-damper-spring system in Fig. 4 consider the step responses shown in Fig. 6, which are obtained for different (dimensionless) active damping gains $\bar{\zeta} \in \{0.05, 1, 5\}$, where $\bar{\zeta} = \beta/(2m\sqrt{k/m})$. In the examples, the system parameter

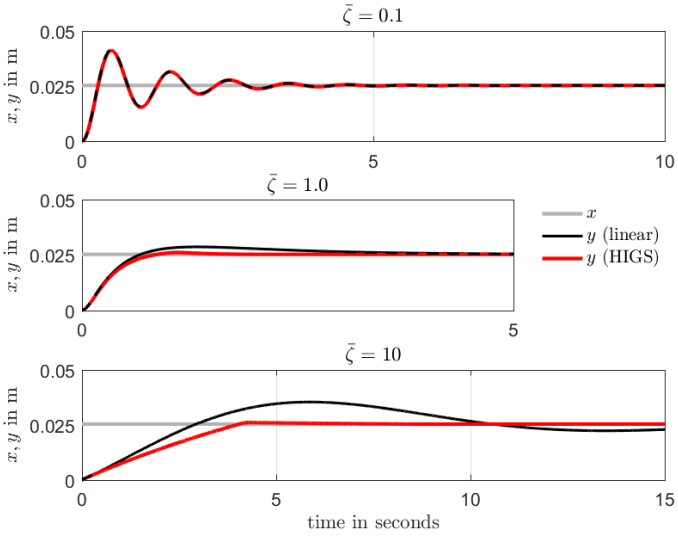

Fig. 6. Time series simulations of the output u of a linear bandpass filter in (10) (dashed-black) and the HIGS-based bandpass filter from Fig.1 (red) to a step input (gray).

values are chosen as $m = 1$ kg, $k = m \times (2\pi)^2$ N/m, and $b = 2m\sqrt{k/m}\zeta$, with $\zeta = 0.05$ the dimensionless passive damping coefficient. Remark that the suspension frequency $\omega_s = \sqrt{k/m}$ corresponds to the design of $\mathscr{H}_{bp}$ and its parameters $\omega_{h,1}, \omega_{h,2}$, the latter being based on $\omega_{lp} = \omega_s/10$ and $\omega_{hp} = 10\omega_s$. For a unity step in x, the response y shows identical behavior for $\bar{\zeta} = 0.1$ regarding linear and HIGS-based skyhook damping. For the larger values $\bar{\zeta} = 1$ and $\bar{\zeta} = 10$, the HIGS-based control design demonstrates responses with less overshoot, faster settling times, but possibly slower rise times.

These observations are confirmed by the more detailed parameter studies underlying Fig. 7. The upper part of the figure depicts overshoot as the percentage by which the largest value $|y(t_o)|$ exceeds the final value $y(t_f)$ with t_o denoting the time instant when the maximum response occurs on $t \in [0, t_f)$ with t_f the final time instant. The middle part considers rise time being the first time instant t_r on $t \in [0, t_f)$ where $|y(t_r)| \leq 0.9|y(t_f)|$, *i.e.*, where $y(t)$ reaches 90% of its final value $y(t_f)$ for the first time. The lower part considers settling time being the time instant $t_s \in [0, t_f)$ after which $|y(t)|$ remains within 5% of its final value $|y(t_f)|$ for $t > t_s$. From Fig. 7, the following

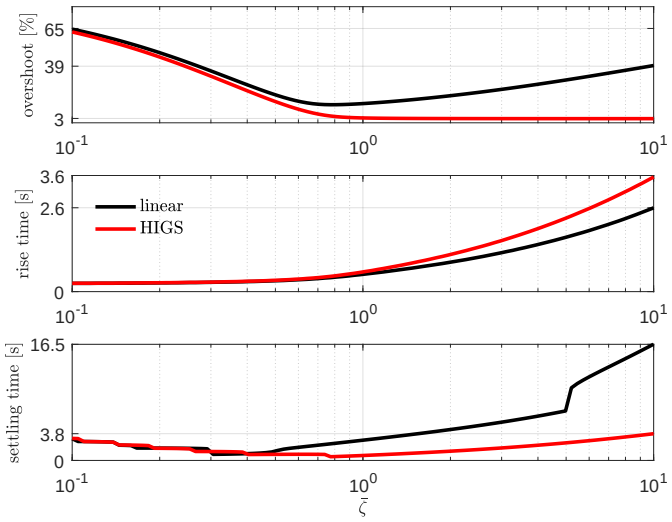

Fig. 7. Parameter studies for different values of the dimensionless skyhook gain $\bar{\zeta} \in [0.1, 10]$.

observations can be made. The HIGS-design only seems effective for sufficiently large skyhook gain values $\bar{\zeta}$. For small values of $\bar{\zeta}$ both the linear and the HIGS-based control design show similar transient behavior in the considered metric. For $\bar{\zeta} > 0.5$ improvements in overshoot as a result of the HIGS-based design become apparent. At $\bar{\zeta} = 10$ overshoot is reduced with a factor of ten when compared to the linear control design. While overshoot unequivocally improves when using the HIGS-based design, the rise time, see the middle part of the figure, deteriorates. This is the result of upper bounding the integral action by gain in the HIGS design. On the contrary, settling times are significantly reduced, almost by a factor of 4 for an active damping coefficient of $\bar{\zeta} = 10$. Note that in high-precision mechatronics rise times are less important than settling times. Also note that for the example, it does not seem useful to use $\bar{\zeta} > 1$ as the overshoot is already minimal at $\bar{\zeta} = 1$ and the rise and settling times only worsen for larger values.

6. CONCLUSION

This paper discusses a hybrid control design for applying active skyhook damping in a vibration isolation context. For large enough required active damping values, typically beyond dimensionless damping coefficient values of 0.5, the hybrid control design leads to reduced overshoot and settling times. For small active damping values, where both linear as well as hybrid control yields comparable performance, one can better reside to linear control design as to avoid introducing unnecessary complexity. Though overshoot and settling times generally improve by using the hybrid control design, rise time unequivocally deteriorates as a result of the hybrid control design itself in which the output of its integrators is always upper-bounded by a gain times its input. Future work will focus on an experimental demonstration. Also, the observation that the HIGS design seems able to avoid frequency-domain deterioration due to phase lag associated with the linear filter design, *i.e.*, a manifestation of Bode's sensitivity integral, will be further examined.

REFERENCES

W.H.T.M. Aangenent, G. Witvoet, W.P.M.H. Heemels, M.J.G. van de Molengraft and M. Steinbuch. Performance analysis of reset control systems, *International Journal of Robust and Nonlinear Control*, DOI: 10.1002/rnc, 2009.

O. Beker, C.V. Hollot, Y. Chait and H. Han. Fundamental properties of reset control systems. *Automatica*, 40, pages 905-915, 2004.

M.A. Beijen, R.J. Voorhoeve, M.F. Heertjes, T.A.E. Oomen. Experimental estimation of transmissibility matrices for industrial multi-axis vibration isolation systems. *Mechanical Systems and Signal Processing*, 107, pages 469-483, 2018.

J. Carrasco, A. Baños and A. van der Schaft. A passivity-based approach to reset control systems stability. *Systems & Control Letters*, 59, pages 18-24, 2010.

D.A. Deenen, M.F. Heertjes, W.P.M.H. Heemels, and H. Nijmeijer. Hybrid integrator design for enhanced tracking in motion control. *In Proceedings of the American Control Conference*, accepted for publication, 2017.

A. Feuer, G.C. Goodwin and M. Salgado. Potential Benefits of Hybrid Control for Linear Time Invariant Plants. *In Proceedings of the American Control Conference*, pages 2790-2794, 1997.

M.F. Heertjes, N. Irigoyen Perdiguero, and D.A. Deenen, Robust data-driven tuning of a hybrid integrator-gain system, International Journal of Adaptive Control and Signal Processing, DOI: 10.1002/acs.2888, 2018.

H. Li and R. Goodall. Linear and non-linear skyhook damping control laws for active railway suspensions. *Control Engineering Practice*, 7(7), pp. 843–850, 1999.

S.J.L.M. van Loon, K.G.J. Gruntjens, M.F. Heertjes, N. van de Wouw, and W.P.M.H. Heemels. (2017) Frequency-domain tools for stability analysis of reset control systems, Automatica, 82, pp. 101-108.

D. Nešić, L. Zaccarian, and A.R. Teel. Stability properties of reset systems. *Automatica*, 44, pages 2019-2026, 2008.

T.A.E.Oomen, R. van Herpen, S. Quist, M.M.J. van de Wal, O.H. Bosgra, and M. Steinbuch, Connecting system identification and robust control for next-generation motion control of a wafer stage, *Transactions on Control Systems Technology*, 22(1), pp. 102–118, 2014.

A. Pavlov, B.G.B. Hunnekens, N.van de Wouw, and H. Nijmeijer. Steady-state performance optimization for nonlinear control systems of Lur'e type, *Automatica*, 49, pp.2087–2097, 2013.

T. van der Poel, J. Van Dijk, B. Jonker, H. Soemers. Improving the vibration isolation performance of hard mounts for precision equipment, *IEEE/ASME international conference on Advanced intelligent mechatronics*, pp.1–5, 2007.

A.Preumont. Vibration control of active structures: an introduction, third edition. Springer, Berlin Heidelberg, Germany, 2011.

S. Skogestad, and I. Postlethwaite. Multivariable feedback control: analysis and design, second edition. Wiley, Chichester, West Sussex, England, 2005.

E.D. Sontag, and Y. Wang. (1995) On characterizations of the input-to-state stability property. *Systems & Control Letters*, 24(5), pp. 351–359.

D. Tjepkema, J. van Dijk, H. Soemers. Sensor fusion for active vibration isolation in precision equipment. *Journal of Sound and Vibration*, 331(4), pp. 735–749, 2011.

L. Zaccarian, D. Nešić, and A.R. Teel. Analytical and numerical Lyapunov functions for SISO linear control systems with first-order reset elements. *International Journal of Robust and Nonlinear Control*, 21, pages 1134-1158, 2011.

Y. Zheng, Y. Chait, C.V. Hollot, M. Steinbuch and M. Norg. Experimental demonstration of reset control design. *Control Engineering Practice*, 8, pages 113-120, 2000.